Title: Abnormal stiffness behaviour in artificial cactus-inspired reinforcement materials

Ioannis Zampetakis[a,b], Yousef Dobah[a], Dong Liu[c], Ben Woods[a], Abderrezak Bezazi[d], Adam Perriman[b], Fabrizio Scarpa[a,*]

[a]Bristol Composites Institute (ACCIS), University of Bristol, BS8 1TR Bristol, United Kingdom

[b]School of Cellular and Molecular Medicine, University of Bristol, BS8 1TD Bristol, United Kingdom

[c] School of Physics, HH Wills Physics Laboratory,Tyndall Avenue, University of Bristol, BS8 1TL Bristol, United Kingdom

[d]Laboratoire de Mécanique Appliquée des Nouveaux Matériaux (LMANM), Université 8 Mai 1945 – Guelma, Algeria

Corresponding authors: f.scarpa@bristol.ac.uk, ioannis.zampetakis@bristol.ac.uk

Abstract

Cactus fibres have previously shown unusual mechanical properties in terms of bending and axial stiffness due to their hierarchical structural morphology. Bioinspiration from those cactus fibres could potentially generate architected materials with exciting properties. To that end we have built bioinspired artificial analogues of cactus fibres to evaluate their mechanical properties. We have generated 3D printed specimens from rendered models of the cactus structure using two different printing techniques to assess the reproducibility of the structural topology. Bioinspired additive manufactured materials with unusual mechanical properties constitute an ever-evolving field for applications ranging from novel wing designs to lightweight plant-inspired analogues. The cactus-inspired 3D printed specimens developed here demonstrate an unusually high bending to axial stiffness ratios regardless of the manufacturing method used. Moreover, when compared to their equivalent beam analogues the cactus specimens demonstrate a significant potential in terms of specific (weight averaged) flexural modulus. Imaging of the artificial cactus reinforcements has enabled the generation of a one-dimensional reduced order finite element model of the cactus structure, with a distribution of cross sections along the length that simulate the inertia and mechanical behaviour of the cactus topology. The novel bioinspired material structure shows an excellent reproducibility across different manufacturing methods and suggest that the tree-like topology of the cactus fibre could be very suited to applications where high bending to axial stiffness ratios are critical.

Graphical Abstract:

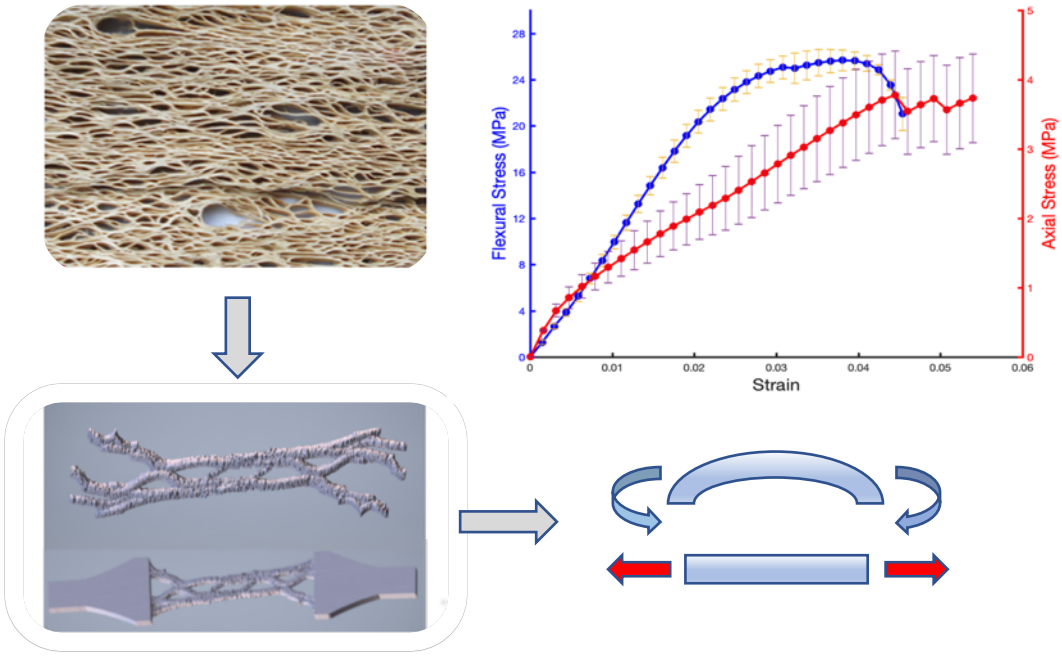

Keywords: cactus, bioinspiration, 3D Printing, Finite Element

Statement of significance

Cactus fibres reinforcements generate unusual bending deformation properties in composite materials. Through the use of μCT and 3D printing artificial cactus fibres have been produced to assess these non-classic structural characteristics and generate novel bioinspired materials. Here we describe a bioinspired cactus-based material platform with high bending to axial stiffness ratios, and also show a set of mechanical simulations and experiments to rationalize this abnormal bending to axial deformation behaviour.

1. Introduction

Nature's material designs have been evolving over large periods of time and tend to feature superior and robust functionalities depending on the specific needs of each organism [1],[2],[3], [40], [41]. Great examples of biological and natural materials that have no direct synthetic counterpart are bone, wood and bamboo. Over the years many attempts have been made to explain and justify the chemical, structural and morphological elements of these biological materials with their unusual properties [3],[4],[42]-[45]. One of the unique advantages of most natural materials is the fact that they are part of a living organism, and they are therefore able to constantly adapt and evolve depending on the environmental context in which they operate. Nature is able to achieve superior and robust functions with very simple constituent materials. The three main reasons generally given in open literature about the optimization and robustness of natural materials lie in the interphase chemistry, structural architectures and the functionality across scales ([3],[5],[42]-[45].). In terms of interphase chemistry, natural materials tend to combine hard and soft constituents in a single interphase and are therefore more efficient to adapt to various loading conditions [6]. As far as structural architectures are concerned, there are eight distinct structural gradients are: i) fibrous, ii) helical iii) gradient iv) layered v) tubular vi) cellular vii) suture and viii) overlapping structures ([7] [32]). Biological materials have the ability to combine and adjust those structural gradients across various scales, while also using multiple ones to optimize functionalities to manage efficiently the different environmental loading scenarios [40]-[45]. The chemical interphase and structural motifs that generate the unique structural, mechanical and multi-functional properties of natural materials have also been observed in various synthetic materials and are common across many material manufacturing methods. The mechanism that potentially provides the most critical contribution for the mechanical development of biological materials

is the presence of functionality across scales, as well as multiscale structural characteristics ([1],[2],[3],[40]-[45]). Advances in imaging techniques have provided a unique insight on the multiscale structural elements of natural materials [7],[41] with an improved understanding of the underlying mechanisms and deformations associated to each structural element at different scales. These imaging techniques have highlighted the fact that through evolution nature performs a continuous optimization and robustness of the morphologies and materials. In particular, an in-depth analysis of biological materials across scales reveals the existence of very interesting architectural features and the prevalence of hierarchical and self-similar structures [1]-[7],[40]-[45] the latter being an attribute of fractal geometry. The existence of hierarchy and self-similarity has been directly related to the mechanical and structural properties of various natural materials. The most common examples are those of bone [8], nacre [6] and bamboo [9], for which it has been demonstrated that the intrinsic hierarchy that exists within the structure leads to global unusual mechanical properties.

The opportunity to deeply understand the phenomena behind the unusual characteristics of natural materials has led to a significant interest in the field of bioinspiration and biomimicry. The word biomimetics first appeared in Webster's dictionary in 1974 [1]. Since then various approaches have been attempted to create materials with chemical morphological and structural features emulating the ones observed in nature ([6], [10]-[14]). As an example, hierarchy is one of the topological reasons behind the 'brick and mortar' structure of nacre that generates the large viscoelastic energy dissipation at the organic mineral level that favours local scale sliding and therefore increase energy absorption and toughness [6],[10]. This understanding of the intrinsic hierarchical characteristics of nacre has enabled the development of bioinspired materials with impressive strength toughness from brittle constituents. Hierarchy has also been observed and biomimicked in glass for novel biocatalytic materials [12],[15],[16].

Various materials have been produced with synthetic routes, however some of the more prevalent techniques used for the generation of bioinspired materials involve additive manufacturing (AM - [17] [18]). The use of AM provides greater opportunities for the development of unique architectures and greater control for the manufactured parts of the structure across scales via artificial porosities and multi-materials printing. The additional levels of manufacturing control introduced by 3D printing make this technique an ideal candidate for the successful replication of unique structures observed in nature, since complicated and hierarchical motifs at different scales can be generated ([15],[19]-[23]). For example, composite materials inspired by the inner structure of osteons, nacre and mantis shrimp have been manufactured via 3D printing. With the bioinspired fibre orientations and placements used, these materials have shown a clear dependence between their macro-mechanical properties and the microarchitecture from 3D print builds [22]. Recently, the microstructure of wood consisting of helical microfibril composites has been observed and reproduced via 3D printing [23]. Plant bioinspiration has led to the development of interesting novel materials through the reproduction of the topological motifs present in plant fibres, while simultaneously providing a unique insight in their unusual structural and mechanical properties [37]. One of those plant fibres that exhibit interesting and unusual mechanical properties are the cladodes of the *Opunita Ficus Indica* (OFI). These cladodes feature an unusual 7:1 bending to axial stiffness ratio that has previously observed experimentally when the cactus fibres were implemented as a polyester matrix reinforcement while also exhibiting significant energy dissipation per volume [24]. An analysis of the anatomy and bio-properties of the OFI reveals that the mechanical properties observed in the cladodes maintain a significant multifunctionality while serving the plant with mechanical performances towards wing loading, protection from herbivores, reflection of light and reduction of the water loss [38], [39]. Those interesting properties demonstrated were attributed to their natural cellular

multiscale fractal-like structure possibly leading to a very interesting bending to axial modulus ratio observed, while also serving essential functions for the plant life [24]. The main focus of this work is the understanding of the structural complexity and the artificial reproduction of the mechanical properties of dried cladodes from *Opuntia ficus indica*; this would enable us to then move towards the development of cactus-inspired materials for structural applications where large bending to axial stiffness modulus ratios are required. The approach used here is similar to a previous methodology employed to characterize the bamboo parenchyma, for which μCT imaging and 3D printing were adopted to explore the mechanical properties of this natural reinforcement [27]. The morphological analysis carried out in our work shows the presence of a hierarchical structure in the cactus fibre across scales. Moreover, the images obtained through CT scanning have been used to generate cactus analogues from different subunits of the original fibre sheath via 3D printing. A reduced order finite element beam model representing the distributions of the moment of inertias on cactus fibres has been developed and benchmarked against the experimental results obtained from the tensile and the 3-point bending tests.

2. Methods

2.1 Extraction of Cactus Fibres

The cactus fibres were extracted as described before [24]. Briefly, *Opuntia Ficus Indica* trunks were buried in sand-less soil 30 cm deep for 15 days with the average outside temperature being at 27ºC where the fermentation process taking place enables the facile removal of the cactus fibre layers. The trunks were then washed with water and left to air dry with outdoor exposure for at least two days at an average temperature of 27ºC. These extracted cactus fibres demonstrating a tree like fibril structure were used for all the analysis described in this work.

2.2 Imaging measurements

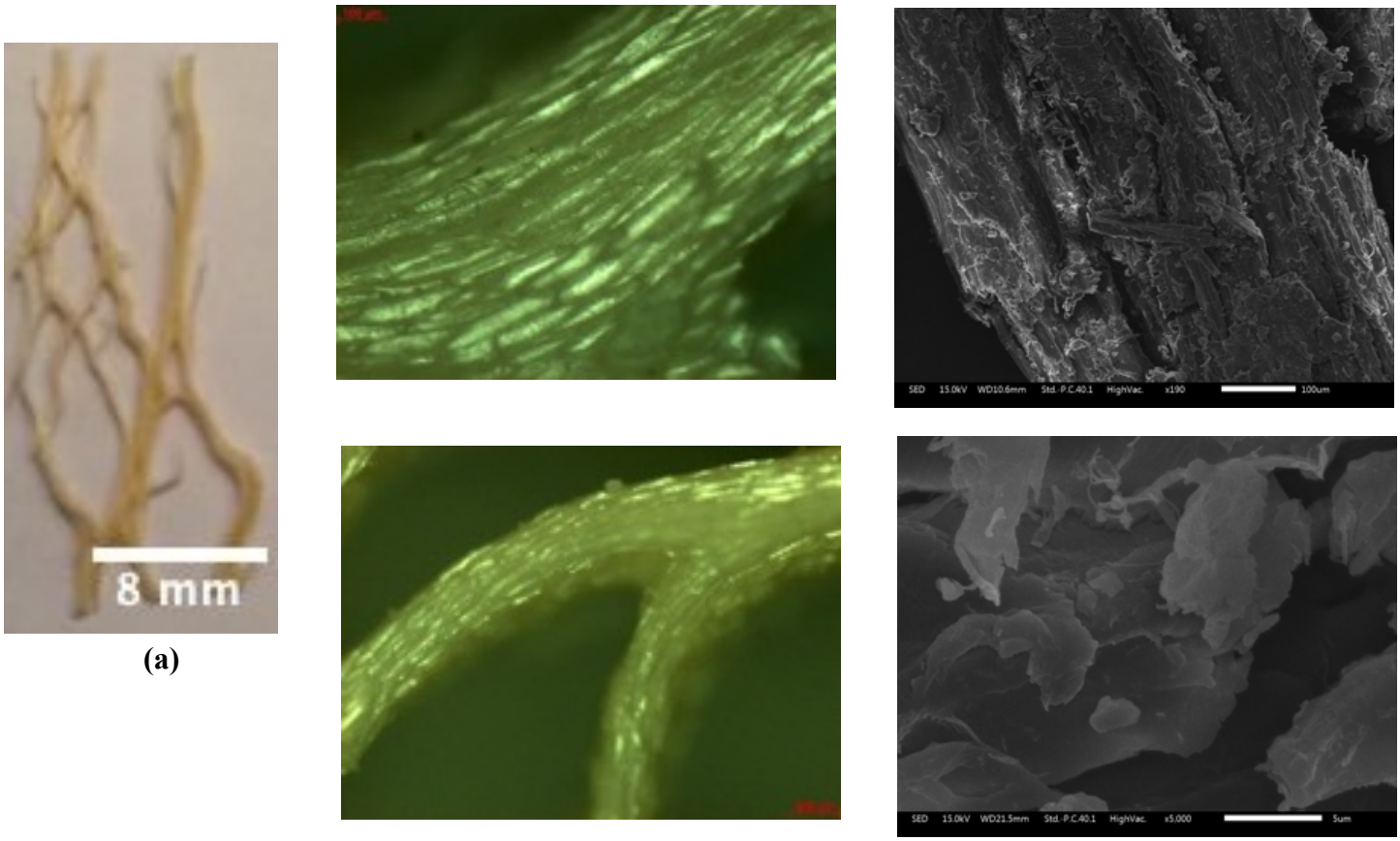

(a) **(b)** **(c)**

Fig. 1. Cactus fibre specimen for X-Ray CT measurements (a), Optical microscopy (b) and SEM (c) images of the original cactus fibres demonstrating the interesting internal and hierarchical structure of the biological material.

X-ray computed micro-tomography scan (μ-CT) was performed on a portion of the cactus sheath (2.5 cm X 2.5 cm X 0.1 cm - Fig. 1a) using a Nikon XTH225ST CT Scanner. The scanning voltage was 35 kV and a 3 X 3 μm voxel size was achieved. Projections were acquired over 360^{o} rotation and the images were reconstructed and viewed using the VG Studio MAX 3.3 software. The μCT data were exported in a tetrahedron mesh .stl from the VG studio MAX software interface using the Polygonal surface Extraction mode; in this study, the iso-gray-value-surface extraction through the auto detect grayvalue method was implemented. The extracted .stl file was then manipulated in Meshlab 2017 to remove non manifold edges and vertices, and also reduce the size of the file by applying the polygon reduction filter via Quadric edge collapse (QEC). This polygon reduction filter was used to significantly reduce the number of polygons in our mesh, since the extraction form the μCT resulted in the extracted mesh having 10^7 polygons, while the printer used in this work could only operate with a maximum of 10^5 polygons. The filter had the option set for the target amount of 10^5 polygons, while maintaining the quality threshold value to 1 for minimizing the modifications made to the overall shape of our model .stl file (a value between 0 to 1 is selected in the filter; the higher the value, the lower the amount of modifications made to the original shape). The use of the polygon reduction filter enabled us to manipulate our .stl file model to generate the 3D printed manufactured specimens. Five additional μCT measurements were performed on the 3D Printed cactus analogue specimens to assess their internal porosity. Optical microscopy images were obtained from a OFI fiber sheet a using a Carl Zeiss Microscope at various magnifications (5x, 10x, 20x) under Bright Field, Dark Field and Polarized Lights settings. SEM images of the fibers were obtained to assess the morphology. The fibre fragments were initially silver coated *via* sputtering using a High-Resolution Sputter Coater (Agar Scientific, UK). Samples were imaged using a JSM IT300 Scanning Electron Microscope (Jeol Ltd., Japan).

2.3 3D Printing

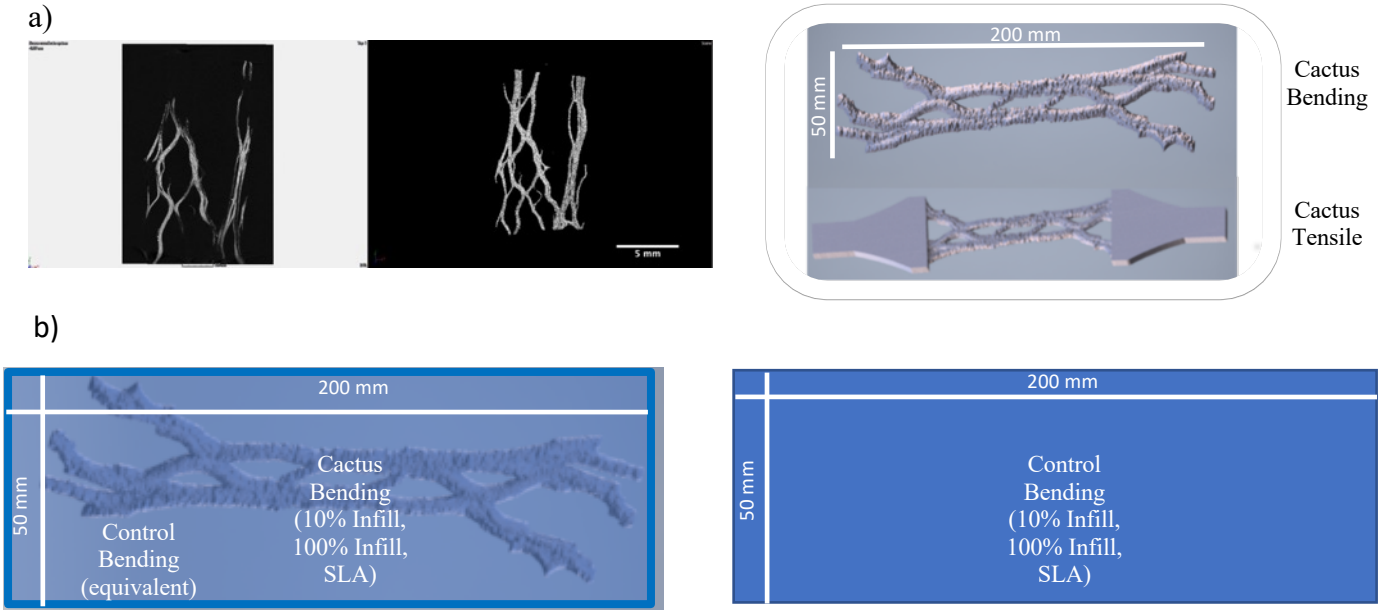

Fig. 2. Design of the 3D printed specimens based on CT images of the cactus fiber structure and those used for the generation of the 3D rendered models for the mechanical testing (a). Graphic representation of the design and conception of the control equivalent specimens used for comparison of the mechanical properties between the cactus structure and an equivalent beam (b).

All PLA samples were printed using Fused Deposition Modelling (FDM) via a Raise 3D N1-V2 Hot End printer with a single roll of Raise 3D Premium PLA filament red. The printing parameter were set at 10% and 100% of infill for the entire model. The two infill values were used to assess geometrical and mechanical differences when changing the internal porosity of the printed part; accordingly, control specimens were printed following the same specifications, using full supports and raft material. Additionally, a 0.2 mm layer height was used at a 30 mm/s speed for the infill and a 60mm/s for the support while the right extruder was used for all prints at 225ºC and a heated bed at 65ºC. The printing parameters were the optimized parameters for the Raise 3D NI-V2 hot end printer as specified by the manufacturer. The SLA specimens were fabricated using a Form 2 SLA printer with Clear Resin V2. All the

supports were used at a layer thickness of 0.1 mm and the post processing was carried out as instructed by the manufacturer.

The samples were initially designed to broadly follow the overall dimensions prescribed by the ASTM standards. That meant that our 3D analogues would have needed a substantially larger thickness than the one observed in the biological material. We have however performed a series of normalizations of the experimental data for the cactus-like samples for a benchmarking of their mechanical properties. We have also compared the 3D printed cactus analogues against ASTM standard control specimens made with bulk polymeric material. Therefore, three categories of specimens have been generated as described in Table 1.

Table1

Tensile & Bending Testing Specimen Dimensions for Analysis

	Length (mm)	Width (mm)	Thickness (mm)	Support Span (mm)	Gage Length (mm)
Cactus_Tensile	200	50	4	-	105
Control_Bending	200	50	4	64	-
Cactus_Bending	200	50	4	64	-

It is important to note that in this approach the cactus structure as a whole was adjusted to match the dimensions required by the ASTM standards. The Cactus_Bending type was therefore a cactus fibre rendered model specifically generated following the ASTM specifications; similarly, the Cactus_Tensile specimen was produced as a cactus structure analogue with ASTM tensile grips attached at the ends.

2.4 Normalization Formulas

In order to compare the mechanical properties between the cactus analogues and the equivalent control beams a density normalization was implemented to generate the specific moduli of the specimens. The formula used was:

$$\text{Specific Modulus (MPa/(g/cm}^3\text{))} = \frac{Flexural\ Modulus}{Density}$$

where the Flexural Modulus is calculated according to ASTM D790-17. To estimate density in our case we used the mass of each control and cactus specimen, and we assumed the volume of the control and cactus specimens to be the same as the control beams were designed to mirror the dimensions of the cactus structure.

2.5 Mechanical Testing

All the tensile tests were carried out according to ASTM D638-14 and all the bending tests were carried out according to ASTM D790-17. A Shimadzu universal testing machine was used fitted with 1 kN Load Cell at a cross bar speed of 1 mm/min both for the tensile and bending tests. No additional equipment was used.

2.6 Finite Element Model

Finite element simulations are in general instrumental in providing further understanding of the mechanisms present in the structure responsible for the mechanical properties observed. In this work we were focusing on the stiffness of a larger scale representation of the cactus structure manufactured with an isotropic material (PLA) and directly compared to an equivalent beam. A linear elastic beam element model representing the distribution of the moment of inertia of the beam was therefore deemed as a reasonable approach to carry out simulations focused on the stiffness characteristics, especially at small strains. A full-scale model representing the complexity of the cactus structure via the wealth of the morphological data obtained from the μCT measurements was initially developed, however computing power available and convergence issues did not enable the meshing of the whole cactus structure. By observing the structure of the 3D printed manufactured cactus specimens, it is evident that the major structural element that is varied across the structure is the cross-sectional area of the specimens. Thus, sections were obtained from the cactus specimen structure to recreate a varying cross-sectional area beam reproducing the same distributions of cross sections

observed in the cactus 3D printed specimens. The model developed could be considered in a sense emulating a coarse-graining approach for the recreation of the structure with the finite element environment. The generation of the Finite element (FE) model was carried out in an ANSYS environment. Initially, morphological information of the 3D printed cactus analogues was obtained in Meshlab 2017, in which sections were obtained and the morphological information of each used for the generation of the equivalent beam. Sections of the cactus configurations were therefore used for the generation of a reduced order model finite element beam, with the number of sections optimized to obtain an acceptable convergence of the model with the experimental data. A non-linear Newton-Raphson solver was used for the bending and tensile loading simulations. It is important to note that only linear elastic properties of the PLA polymer were used here for the FE material selection. Those properties were evaluated *via* a ASTM D638-14 tensile test and it was determined that the experimental values matched closely the elastic properties specified by the manufacturer. The finite element model had the two ends represented by clamps (i.e., no translational or rotational degrees of freedom allowed). To account for the macro-porosity present in the cactus structure, an infill factor was introduced in the material constants of the model to account for the effective porosity present due to the 3D printing infill and also the complexity of each cross section utilized.

3. Results

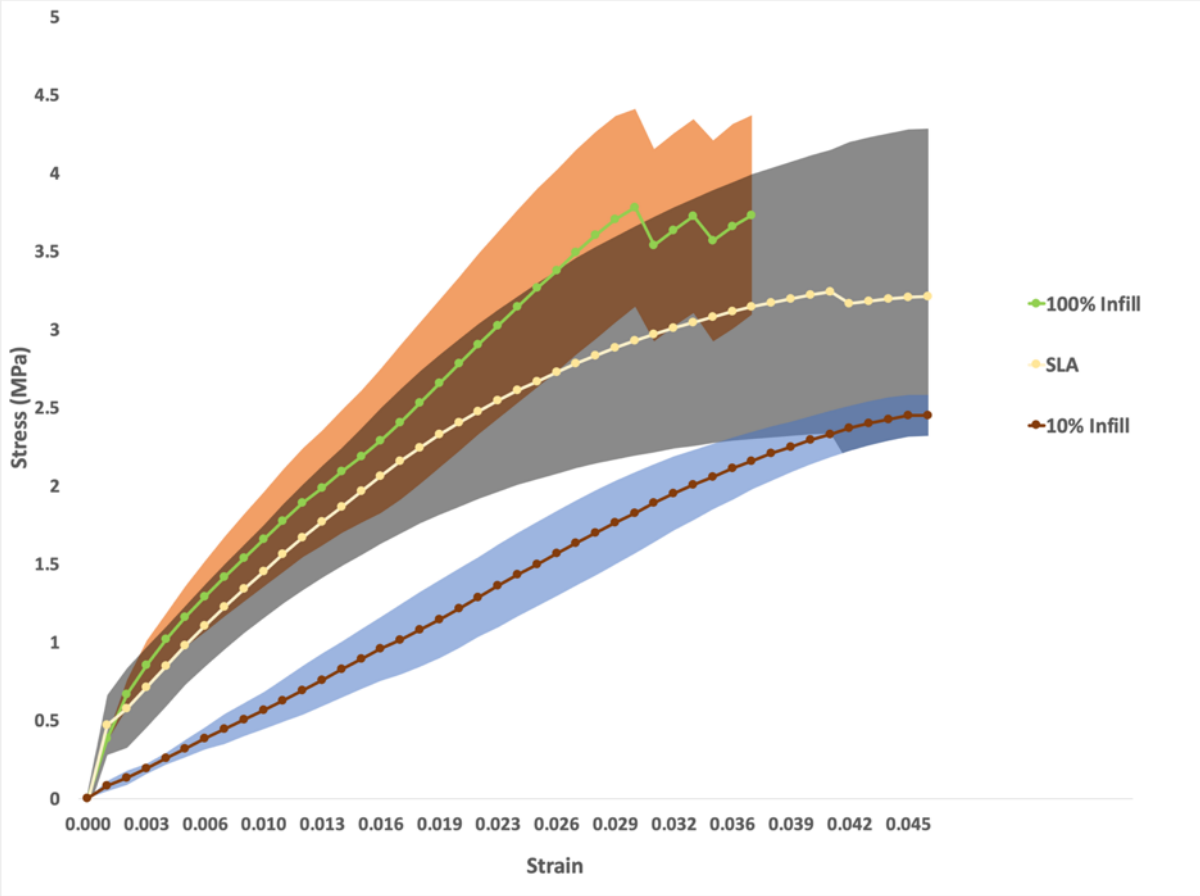

Fig. 3. Tensile Testing results according to ASTM D638-14 for 10% infill PLA, 100% infill PLA & SLA, with the standard deviation depicted as a colour-shaded area. (n=5)

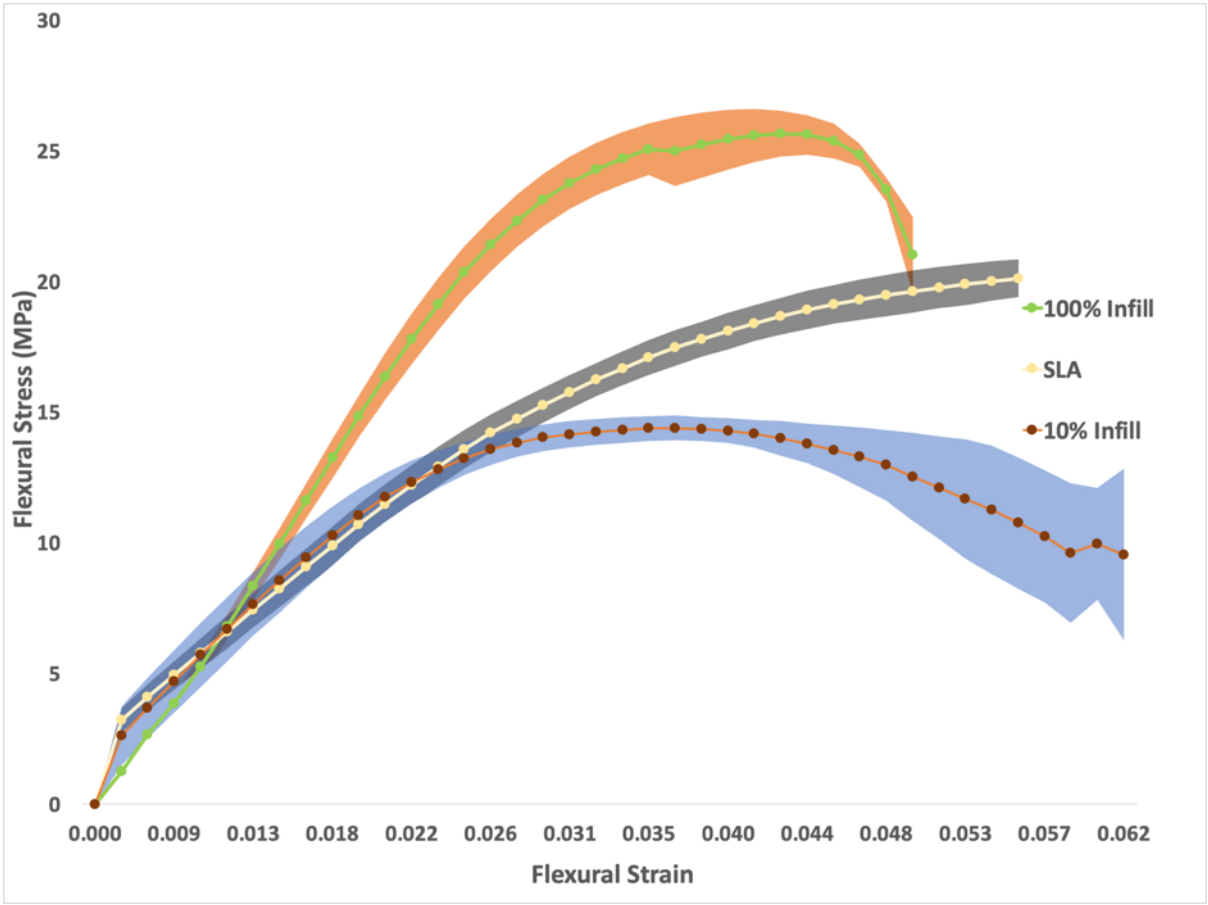

Fig. 4. Bending Testing results according to ASTM D790-17 for 10% infill PLA, 100% infill PLA & SLA, with the standard deviation depicted as a colour-shaded area (n=5).

Table 2

Axial and Flexural Modulus of all specimens and equivalent bending to axial stiffness ratio. The designs are described in detail in Fig. 2b. The different infill ratios used prove that, irrespective of the internal structure of the specimens, the high stiffness ratio is maintained. The percentages correspond to infill percent utilized in the case of the PLA 3D printing. Specimen Manufacturing according to Fig. 2.

	Axial Modulus (MPa)	Flexural Modulus (MPa)	Ratio
Cactus_10%_PLA	60.5 ± 10 .2	602.2± 13.4	9.9
Cactus_100%_PLA	102 ± 14	1025.5 ± 44.3	10
Cactus_SLA	120.7 ± 15.5	581.7 ± 37.4	5

Table 3

Mass, Volume and Density measurements for all test specimens. Percentages correspond to infill percent utilized in the case of the PLA 3D printing. Specimen Manufacturing according to Fig. 2.

	Mass (g)	Volume (cm^3) (Equivalent Beam)	Density (g/cm^3)
Control_PLA_10%	22.2 ± 0.03	40	0.55
Cactus_PLA_10%	13.4 ± 0.02	40	0.34
Control__PLA_100%	47.6 ± .3	40	1.2
Cactus__PLA_100%	21.4 ± 0.1	40	0.54
Control_SLA	51.1 ± 0.2	40	1.3
Cactus_SLA	21.6 ± 0.3	40	0.54

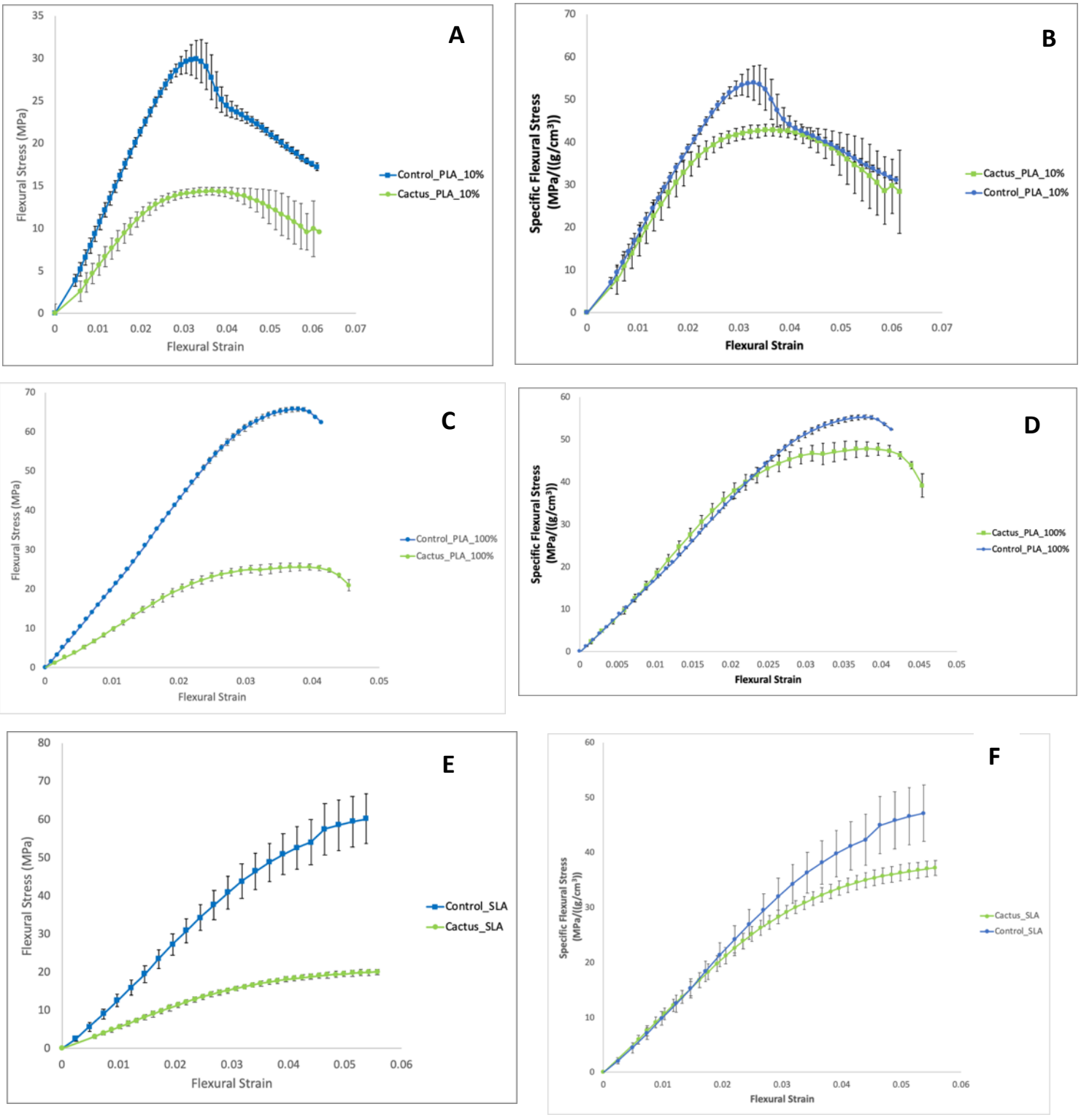

Fig. 5. Flexural Stress compared with Specific Flexural stress for 10 % PLA (a), (b), 100 % PLA (c), (d), SLA PLA (e), (f). ASTM D790-17 (n=5)

Table 4

Flexural and specific flexural moduli of all specimens. No significant difference is observed between the Controls and cactus Equivalents for each specimen category (t-test, $p<0.05$)

	Flexural Modulus (MPa)	Specific Flexural Modulus (MPa/(g/cm^3))
Control_PLA_10%	1079 ± 4	1944.3 ± 42.5
Cactus_PLA_10%	602.2 ± 13.4	1939.6± 55.1
Control_PLA_100%	2154.6 ± 27.8	1856.4± 54
Cactus_PLA_100%	1025.5 ± 44.3	1923.8± 94.3
Control_SLA	1194.9 ± 125	1132.7± 97.7
Cactus_SLA	581.7 ± 37.4	1045.4± 49.4

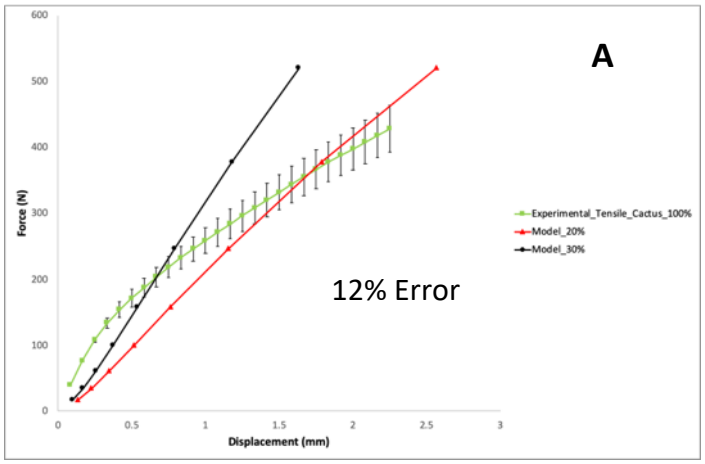

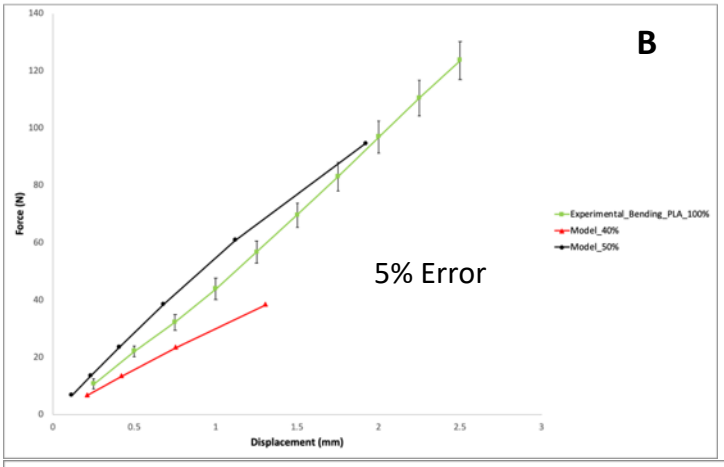

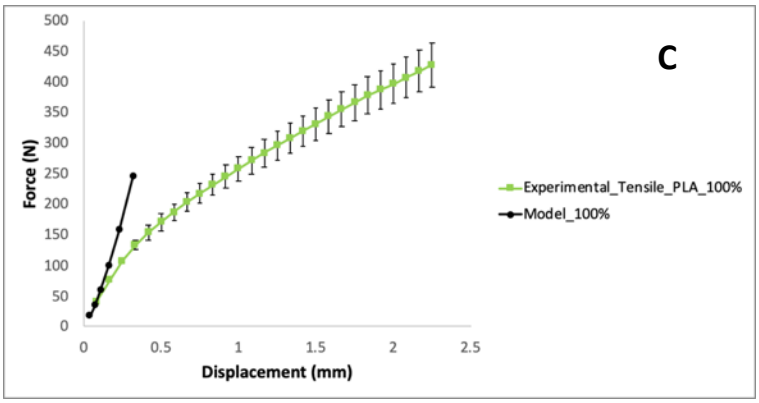

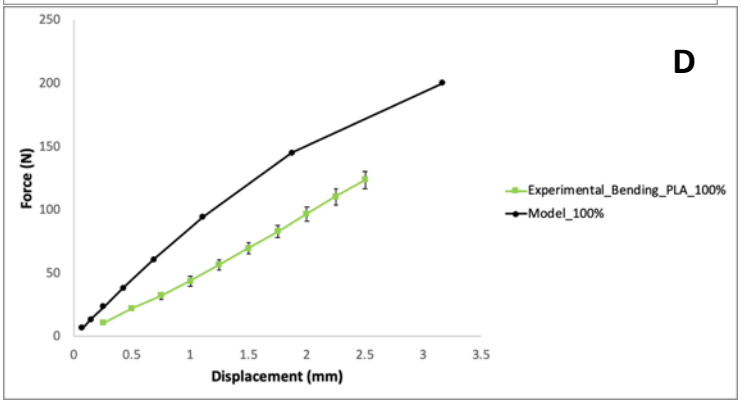

Fig. 6. Finite Element Simulations results for 100% PLA in Tensile at 20 and 30% Percent infill (a), 100% PLA in Bending in 40 and 50% infill (b), 100% PLA in Tensile 100% PLA in Tensile at 100% Infill (c), 100% PLA in Bending in 40 and 50% infill (d)

Table 5

Finite element simulations predicted modulus at 100% Infill

	Tensile Modulus (MPa)	Flexural Modulus (MPa)	Ratio
FE_100%_PLA	377.3	1589.4	4.2

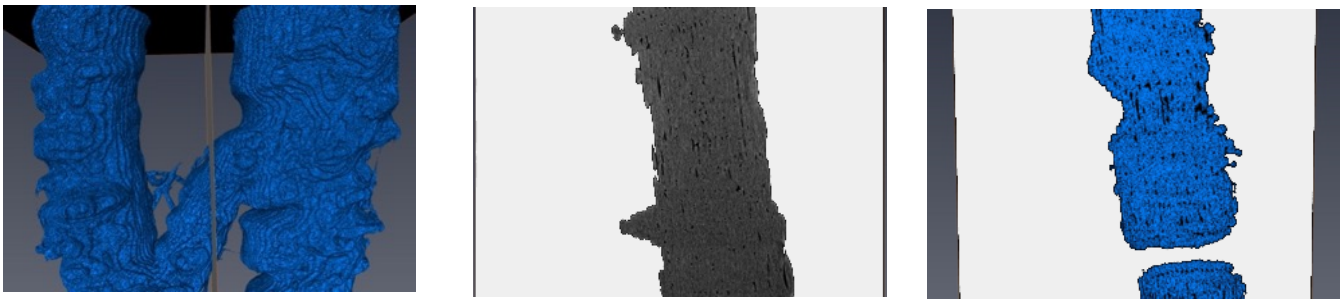

Fig. 7. µCT results of the 3D Printed cactus analogues at 100% PLA infill demonstrating the porosity throughout the structure.

4. Discussion

4.1 Cactus Inspired 3D Printed analogues

In this work we have aimed at artificially reproducing cactus fibre cellular structures that have previously shown an unusual 7:1 bending to axial stiffness ratio. For this purpose, we have used various materials and manufacturing methods. Through μCT measurements we were able to generate 3D rendered models and export triangular meshes of the cactus structure that were then further optimized and manipulated to produce 3D printed specimens maintaining the structural integrity of the cactus structure, as much as possible, as evident in Fig.2. Once the STL files of the cactus structure were optimized for 3D printing through fixing all the nonmanifold edges and vertices, they were 3D printed with two different printing modalities. Initially the cactus structures were produced using a commercial FDM 3D printer using commercial PLA filament at two different infill ratios (10% and 100%). The different infills were used to determine their effect on the mechanical characteristics of the structure, as well as to understand if the bending to axial stiffness ratio would be maintained irrespectively of the amount of material used. It is also important to note that the specimens manufactured are at a much larger scale than the original cactus specimen. The purpose of doing this was twofold. The first was to generate specimens that would be conforming with the ASTM standards, so to compare the cactus analogues with other materials and with control specimens of equivalent beams. The second justification, behind the choice of making larger specimens, was to verify the presence of any scale issue, and that the architectural and geometric structures present in the fibres are responsible for the unusual bending/axial ratio observed in nature. As evident from observing Figs.3, 4 and Table 2, the high bending to axial stiffness ratio in these artificial cactus fibre-inspired structures varies between 9.9:1 and 10:1 for the 10 % and 100% infill specimens, respectively. Those bending to axial stiffness rations are slightly higher than the one observed in nature, however this can be also attributed to the added-on tabs of the

specimens used for the gripping during the tensile tests; the grips could introduce a source of error on our measurements, together with a slightly higher degree of tensile compliance. To ensure the reproducibility of those results irrespective of the materials and manufacturing methods used, the same specimens were manufactured by stereolithography. The specimens manufactured with the SLA printing method were produced with the same specifications as the ones for the PLA printed specimens. Also, in this case (see Figs. 3 and 4), a high bending to axial stiffness ratio is observed, and this value is closer to the 7:1 observed in the biological material. This could be attributed to the higher printing resolution of the stereolithography method as compared to the FDM one [31].

4.2 Understanding of the Cactus Fibre Structure

Notwithstanding the manufacturing method used, the fact that the high bending to axial stiffness is present in all the specimens produced provides additional supporting evidence that the tree-like geometry characteristics of the cactus fibre sheaths are the primary driver behind the unusual bending to axial stiffness ratio behaviour. Hierarchical fractal-like configurations generate materials with significant mechanical benefits in comparison to non-hierarchical structures [32], and the fractal-like configuration of the cactus fibre appears to provide another set of unusual mechanical properties. To the Authors' knowledge this is the first structure that demonstrates this unusual deformation mechanism. Previously reported natural fibre bio composites do possess significantly high bending to axial stiffness ratios: wood (4:1), arabaca (5:1) and jute fibres (5:1). Single carbon fibres also show very high bending to axial stiffness ratios (9:1), however this is due to the direction of loading with respect to the fibre alignment in the matrix [25],[28],[29]. In the cactus structure this behaviour is generated by a single component material that appears to be replicated and maintained in these tree-like morphologies, irrespective of the material and manufacturing method used. A direct comparison with the control specimens in FDM and SLA (Fig.5) shows that those bulk solid

samples demonstrate a significantly higher flexural modulus when compared to the cactus 3D printed analogues. However, one the biggest benefits of cellular materials is their macro porosity, which enables a weight reduction allows some excellent mechanical performance in terms of specific (density averaged) stiffnesses [26]. Once the density normalization is performed (Table 3) it is evident in Fig.5 that the cactus specific flexural modulus is directly comparable to that of an equivalent beam. This demonstrates the significant potential of the cactus structure in applications where a high bending modulus per unit weight is required. The cactus structure, at half the weight of its equivalent beam generates a directly comparable flexural modulus.

4.3 Finite Element Simulations

A more in-depth understanding of the behaviour of these materials could however be only achieved through the development of mechanical simulations. In the original work on cactus fibre polyester composites [24] a modelling approach based on lattice beam constructions was adopted, with the assumption that the hierarchical structure of the cactus fibrils and bundles across scales enables the generation of these high bending to axial stiffness ratios. The model also pointed out that the 'tree-like' structure was responsible at the macro scale of the increased high bending modulus of the cactus fibre sheath. The 3D printed analogues of this work do not have a hierarchical structure present, as they were manufactured through an additive manufacturing method in which the same layer is applied repeatedly to develop the final part. Moreover, the 3D printed analogues are not strictly speaking composite multiphase materials, since they have been developed using a single type of solid. These bio-inspired artificial reinforcement materials have been also generated using a small structural subunit from the whole cactus fibre sheath structure, following the hypothesis of fractal geometry present within the biomaterial. For these reasons the 3D lattice hierarchical model implemented previously could not be used for the characterization of the 3D printed analogue specimens and a new

approach was necessary. A reduced finite element beam that would replicate the cactus geometrical properties was therefore implemented for the simulations. By observing the cactus stl file in Fig. 6 used for the printing of the 3D cactus analogue parts it is evident that the variability of the shape is mainly across the width of the structure. An equivalent beam that would replicate the structural elements of the cactus structure would therefore, at a very fundamental level, be a beam with a varied cross section area and moments of inertia. The infill factor is introduced to accommodate for the effective porosity existing due to the complexity of the cross-sectional areas, as well as the porosity introduced through the 3D printing infilling. The infill factor implemented Fig.6 shows that this approach provides a good approximation of the bending of the cactus analogue, with the one given by the equivalent beam at an infill level of 40-50% yielding an error of 5% when comparing the modulus value between the predicted result from the FE model and the experimental data. Assuming that a solid equivalent beam would have an infill level of 100%, the infill level used of 40-50% translates into an effective porosity in the model of 50-60%. This result is to be expected; as observed in the cactus analogue structure of Fig.2, the macro-porosity of the structure is evident. The mass of the cactus 3D printed analogues is also about half the mass of their equivalent beams generated to replicate the geometrical characteristics of the cactus structures of Tables 1 and 3. Additional evidence of the porosity exhibited in the 3D printed cactus analogue specimen is shown in Fig.7, in which a μCT scan of the 3D printed cactus analogue is presented. One can observe the presence of the internal porosity throughout the structure, which was quantified at 5%. The internal porosity observed within the sections of the 3D printed specimen combined with the macro-porosity present in the cellular cactus structure explains the prediction from the model of the bending properties of the cactus structure at porosities between 50-60%. The more interesting results from the simulations are however related to the prediction of the tensile behaviour of the cactus 3D printed analogues. The predicted tensile behaviour is expected from

a cactus-equivalent beam at an infill of 20-30%, i.e. with porosity of 70-80% (Fig. 6), which is very different than then porosity predicted from the bending simulations while also yielding a significantly higher error in terms of the modulus value obtained between the projected result of the FE model and the experimental data at 12%. The finite element simulations carried out demonstrate that the reduced order model approach alone is not adequate to predict the mechanical behaviour of the cactus structure. However, some useful information about the mechanical properties of the cactus configuration can still be obtained. When the infill is 100% (i.e., no porosity in the equivalent beam), the bending to axial stiffness ratio is around 4 to 1 (see Fig.6 and Table 5). Even though this is still a significantly high bending to axial stiffness ratio, it is lower than the one shown by the cactus structure. It is also interesting to observe that the correct bending to axial stiffness ratio is achieved by the simulation once the porosity of the tensile testing is increased, making therefore the beam significantly compliant in tension as a result of the increased porosity. At the same time, if the same value of porosity is used for the simulation of the bending stiffness the predicted bending modulus is significantly lower than the one of the experimental data. The fact that the structure in bending loading scenarios behaves significantly better than expected means that besides the varied cross- sectional area the architecture of the structure and lower scales and the location and distribution of the pores play a significant role for the mechanical properties observed. The porosity in the finite element simulation is distributed uniformly over the cross sections, whereas in the cactus structure the pores are localized in specific areas, with the outer surface of the samples showing a higher density. That would effectively generate hollow cross sections, with higher thickness close to the external surfaces and therefore higher bending moment of inertia. Moreover, in the tensile loading scenarios the topography of the porosity of the structure serves as a disadvantage, because cellular solids tend to be bending dominated from a mechanical perspective and are significantly more compliant in tension [33]. Although the reduced order finite element model

shows some limits, it does however provide some insight on the architectural and morphological properties present in the cactus structure. The 4:1 ratio obtained by the models at 100% infilling suggests indeed that the geometry of the tree-like configuration provides unusual bending to axial stiffness behaviours, which could find applications in various fields. For example, a high bending to stiffness ratio would be useful in shape morphing applications in aerofoils, in which structures need to be stretched but the shape under bending needs to be preserved [34]. The different stiffnesses in stretching and bending also suggest different strain energy mechanisms being present in the same architecture; this could be used to design structures with tailored energy absorption capabilities that depend on the type of external loading provided [35].

5. Conclusions

Biological materials have always been on the forefront of scientific and industrial focus due to their interesting properties and abundance, while bioinspiration through additive manufacturing has enabled the generation of novel biological based materials with unique properties expanding the material field significantly. Specifically, previous work on cactus fibres has demonstrated that the morphology and architectural characteristics of this fibre when implemented as a matrix reinforcement, yield composite materials with unusual high bending to axial stiffness ratios and a significant increase in energy dissipation per volume matrix. The ability to extensively image the cactus structure in an effort to understand its mechanical properties and explain the presence of this unusual high ratio led to the generation of 3D rendered models of a simplified cactus configurations. Three-dimensional models of the cactus structure from natural fibres sheaths were 3D printed using two different additive manufacturing methods. The 3D artificial cactus analogues were tested in 3-point bending and

tensile loading following the appropriate ASTM standards for plastic parts. The results demonstrated that the high bending to axial stiffness ratio is maintained irrespective of manufacturing method and material used. In some cases the original 7:1 bending to stiffness ratio observed for the cactus natural fibres was surpassed by the artificial cactus surrogates. The cactus fibre hierarchical structure is primarily responsible for the unusual mechanical characteristics. The 3D printed cactus analogues also possessed higher specific bending stiffness when compared to equivalent bulk materials beams with same overall dimensions. Even though the reduced order Finite Element model developed here was not able to fully capture the mechanical properties observed in the cactus printed analogues, it nevertheless allowed to understand the importance of the tree-like architecture in providing the high bending to axial stiffness ratio, especially when samples with complete filling were simulated. Overall, we have demonstrated the ability to use 3D printing for the explanation of some unique structural characteristics observed in a biological material, while also developing a novel bioinspired structural platform with unusual high bending to axial stiffness ratios for multifunctional applications.

Acknowledgements

The work has been supported by Dstl and the EPSRC Centre for Doctoral Training in Synthetic Biology (SynBio). DL acknowledges the support from EPSRC Fellowship grant (EP/N004493/1) and the Royal Commission for the Exhibition of 1851 Fellowship project.

References

1. Bhushan, B. Biomimetics: lessons from nature–an overview. *Philosophical Transactions of the Royal Society A: Mathematical, Physical and Engineering Sciences* **367**, 1445 (2009)
2. Fratzl, P. Biomimetic materials research: what can we really learn from nature's structural materials? *Journal of The Royal Society Interface* **4**, 637 (2007).
3. Wegst, U. G. K., Bai, H., Saiz, E., Tomsia, A. P. & Ritchie, R. O. Bioinspired structural materials. *Nat Mater* **14**, 23-36, doi:10.1038/nmat4089 (2015).
4. Chen, P.-Y., McKittrick, J. & Meyers, M. A. Biological materials: Functional adaptations and bioinspired designs. *Progress in Materials Science* **57**, 1492-1704, doi:https://doi.org/10.1016/j.pmatsci.2012.03.001 (2012).
5. Smith, B. L. *et al.* Molecular mechanistic origin of the toughness of natural adhesives, fibres and composites. *Nature* **399**, 761-763, doi:10.1038/21607 (1999).
6. Munch, E. *et al.* Tough, Bio-Inspired Hybrid Materials. *Science* **322**, 1516, doi:10.1126/science.1164865 (2008).
7. du Plessis, A. & Broeckhoven, C. Looking deep into nature: A review of micro-computed tomography in biomimicry. *Acta Biomaterialia* **85**, 27-40, doi:https://doi.org/10.1016/j.actbio.2018.12.014 (2019).
8. Weinkamer, R. & Fratzl, P. Mechanical adaptation of biological materials — The examples of bone and wood. *Materials Science and Engineering: C* **31**, 1164-1173, doi:https://doi.org/10.1016/j.msec.2010.12.002 (2011).
9. Tan, T. *et al.* Mechanical properties of functionally graded hierarchical bamboo structures. *Acta Biomaterialia* **7**, 3796-3803, doi:https://doi.org/10.1016/j.actbio.2011.06.008 (2011).
10. Bouville, F. *et al.* Corrigendum: Strong, tough and stiff bioinspired ceramics from brittle constituents. *Nature Materials* **16**, 1271, doi:10.1038/nmat4982 (2017).
11. Yoo, S. C., Park, Y. K., Park, C., Ryu, H. & Hong, S. H. Biomimetic Artificial Nacre: Boron Nitride Nanosheets/Gelatin Nanocomposites for Biomedical Applications. *Advanced Functional Materials* **0**, 1805948, doi:10.1002/adfm.201805948 (2018).
12. Mirkhalaf, M., Dastjerdi, A. K. & Barthelat, F. Overcoming the brittleness of glass through bio-inspiration and micro-architecture. *Nature Communications* **5**, 3166, doi:10.1038/ncomms4166 (2014).
13. Fernandez, J. G. & Ingber, D. E. Unexpected Strength and Toughness in Chitosan-Fibroin Laminates Inspired by Insect Cuticle. *Advanced Materials* **24**, 480-484, doi:10.1002/adma.201104051 (2011).
14. Wu, Z. *et al.* Biomimetic structure design and construction of cactus-like MoS2/Bi19Cl3S27 photocatalysts for efficient hydrogen evolution. *Journal of Materials Chemistry A*, doi:10.1039/C8TA08834A (2018).
15. Porter, M. M., Ravikumar, N., Barthelat, F. & Martini, R. 3D-printing and mechanics of bio-inspired articulated and multi-material structures. *Journal of the Mechanical Behavior of Biomedical Materials* **73**, 114-126,
16. Dimas, L. S., Bratzel, G. H., Eylon, I. & Buehler, M. J. Tough Composites Inspired by Mineralized Natural Materials: Computation, 3D printing, and Testing. *Advanced Functional Materials* **23**, 4629-4638, doi:10.1002/adfm.201300215 (2013).
17. Studart, A. R. Additive manufacturing of biologically-inspired materials. *Chemical*

Society Reviews **45**, 359-376, doi:10.1039/C5CS00836K (2016).
18. 1 Hull, C. W. (Google Patents, 1986).
19. Dimas, L. S., Bratzel, G. H., Eylon, I. & Buehler, M. J. Tough Composites Inspired by Mineralized Natural Materials: Computation, 3D printing, and Testing. *Advanced Functional Materials* **23**, 4629-4638, doi:10.1002/adfm.201300215 (2013).
20. de Obaldia, E. E., Jeong, C., Grunenfelder, L. K., Kisailus, D. & Zavattieri, P. Analysis of the mechanical response of biomimetic materials with highly oriented microstructures through 3D printing, mechanical testing and modeling. *Journal of the Mechanical Behavior of Biomedical Materials* **48**, 70-85,
21. Kokkinis, D., Bouville, F. & Studart, A. R. 3D Printing of Materials with Tunable Failure via Bioinspired Mechanical Gradients. *Advanced Materials* **30**, 1705808, doi:10.1002/adma.201705808 (2018).
22. Martin, J. J., Fiore, B. E. & Erb, R. M. Designing bioinspired composite reinforcement architectures via 3D magnetic printing. *Nature Communications* **6**, 8641, doi:10.1038/ncomms9641
https://www.nature.com/articles/ncomms9641#supplementary-information (2015).
23. Zorzetto, L. & Ruffoni, D. Wood-Inspired 3D-Printed Helical Composites with Tunable and Enhanced Mechanical Performance. *Advanced Functional Materials* **29**, 1805888, doi:10.1002/adfm.201805888 (2019).
24. Bouakba, M., Bezazi, A., Boba, K., Scarpa, F. & Bellamy, S. Cactus fibre/polyester biocomposites: Manufacturing, quasi-static mechanical and fatigue characterisation. *Composites Science and Technology* **74**, 150-159, doi:http://dx.doi.org/10.1016/j.compscitech.2012.10.009 (2013).
25. Kim, S.-J., Moon, J.-B., Kim, G.-H. & Ha, C.-S. Mechanical properties of polypropylene/natural fiber composites: Comparison of wood fiber and cotton fiber. *Polymer Testing* **27**, 801-806, doi:https://doi.org/10.1016/j.polymertesting.2008.06.002 (2008).
26. L.J. Gibson, M.F. Ashby, B.A. Harley **Cellular materials in nature and medicine** Cambridge University Press, Cambridge (UK) (2010)
27. Dixon, P. G. *et al.* 3D printed structures for modeling the Young's modulus of bamboo parenchyma. *Acta Biomaterialia* **68**, 90-98, doi:https://doi.org/10.1016/j.actbio.2017.12.036 (2018).
28. Reis, J. M. L., Lima, R. P. & Vidal, S. D. Effect of rate and temperature on the mechanical properties of epoxy BADGE reinforced with carbon nanotubes. *Composite Structures* **202**, 89-94, doi:https://doi.org/10.1016/j.compstruct.2017.11.081 (2018).
29. Vijaya Ramnath, B. *et al.* Evaluation of mechanical properties of abaca–jute–glass fibre reinforced epoxy composite. *Materials & Design* **51**, 357-366, doi:https://doi.org/10.1016/j.matdes.2013.03.102 (2013).
30. Naleway, S. E., Porter, M. M., McKittrick, J. & Meyers, M. A. Structural Design Elements in Biological Materials: Application to Bioinspiration. *Advanced Materials* **27**, 5455-5476, doi:10.1002/adma.201502403 (2015).
31. Bhushan, B. & Caspers, M. An overview of additive manufacturing (3D printing) for microfabrication. *Microsystem Technologies* **23**, 1117-1124, doi:10.1007/s00542-017-3342-8 (2017).
32. Meza, L. R. *et al.* Resilient 3D hierarchical architected metamaterials. *Proceedings of the National Academy of Sciences* **112**, 11502, doi:10.1073/pnas.1509120112 (2015).
33. Ronan, W., Deshpande, V. S. & Fleck, N. A. The tensile ductility of cellular Solids: The role of imperfections. *International Journal of Solids and Structures* **102-103**, 200-213, doi:https://doi.org/10.1016/j.ijsolstr.2016.10.004 (2016).

34. Heo, H., Ju, J. & Kim, D.-M. Compliant cellular structures: Application to a passive morphing airfoil. *Composite Structures* **106**, 560-569, doi:https://doi.org/10.1016/j.compstruct.2013.07.013 (2013).
35. DiPalma, M. & Gandhi, F. in *24th AIAA/AHS Adaptive Structures Conference AIAA SciTech Forum* (American Institute of Aeronautics and Astronautics, 2016).
36. Sullivan, T. N., Hung, T.-T., Velasco-Hogan, A. & Meyers, M. A. Bioinspired avian feather designs. *Materials Science and Engineering: C* **105**, 110066, doi:https://doi.org/10.1016/j.msec.2019.110066 (2019).
37. Kaminski, R., Speck, T. & Speck, O. Biomimetic 3D printed lightweight constructions: a comparison of profiles with various geometries for efficient material usage inspired by square-shaped plant stems. *Bioinspiration & Biomimetics* **14**, 046007, doi:10.1088/1748-3190/ab202f (2019).
38. Stintzing, F. C. & Carle, R. Cactus stems (Opuntia spp.): A review on their chemistry, technology, and uses. *Molecular Nutrition & Food Research* **49**, 175-194, doi:10.1002/mnfr.200400071 (2005).
39. Anderson, E. F., The Cactus Family, Timber Press, Portland, OR 2001, pp. 15 –72.
40. Jeronimidis, G. & Atkins, A. G. Mechanics of Biological Materials and Structures: Nature's Lessons for the Engineer. *Proceedings of the Institution of Mechanical Engineers, Part C: Journal of Mechanical Engineering Science* **209**, 221-235, doi:10.1243/PIME_PROC_1995_209_149_02 (1995).
41. Lakes, R. Materials with structural hierarchy. *Nature* **361**, 511-515 (1993).
42. National Research, C. *Hierarchical Structures in Biology as a Guide for New Materials Technology*. (The National Academies Press, 1994).
43. Sarikaya, M. An introduction to biomimetics: a structural viewpoint. *Microscopy research and technique* **27**, 360-375 (1994).
44. Srinivasan, A. V., Haritos, G. K. & Hedberg, F. L. Biomimetics: Advancing Man-Made Materials Through Guidance From Nature. *Applied Mechanics Reviews* **44**, 463-482, doi:10.1115/1.3119489 (1991).
45. Weiner, S. & Addadi, L. Design strategies in mineralized biological materials. *Journal of Materials Chemistry* **7**, 689-702 (1997).